



Cite this: *J. Mater. Chem. A*, 2023, **11**, 6299

## Active $\text{BaTaO}_2\text{N}$ photocatalysts prepared from an amorphous $\text{Ta}_2\text{O}_5$ precursor for overall water splitting under visible light†

Shinji Nishimae,<sup>a</sup> Junie Jhon M. Vequizo,<sup>b</sup> Yasunobu Inoue,<sup>a</sup> Akira Yamakata,<sup>b</sup> Mamiko Nakabayashi,<sup>d</sup> Tomohiro Higashi,<sup>e</sup> and Kazunari Domen<sup>a</sup>                                            

Barium tantalum oxynitride ( $\text{BaTaO}_2\text{N}$ ), a photocatalyst active during one-step-excitation overall water splitting under visible light, was synthesized by  $\text{NH}_3$ -based nitridation of a mixture of  $\text{BaCO}_3$  and amorphous  $\text{Ta}_2\text{O}_5 \cdot 3\text{H}_2\text{O}$ .  $\text{H}_2$  and  $\text{O}_2$  were generated from water in stoichiometric amounts and in a stable manner using this material modified with Rh (or Ru),  $\text{Cr}_2\text{O}_3$  and  $\text{IrO}_2$  cocatalysts. This photocatalyst was responsive to visible light up to a wavelength of 540 nm for the water splitting reaction. Trials using nitridation temperatures from 1023 to 1273 K and durations from 0.5 to 20 h indicated that mild nitridation conditions such as 1123 K and 5 h provided high-performance specimens, whereas prolonged nitridation (15–20 h) dramatically decreased the photocatalytic activity. Transient absorption spectroscopy showed that  $\text{BaTaO}_2\text{N}$  generated abundant photoexcited free electrons with long lifetimes due to a low concentration of defects such as oxygen vacancies, but was deactivated after prolonged nitridation. X-ray photoelectron spectra indicated that overly long nitridation generated recombination sites such as  $\text{Ta}^{3+}$ . The mechanism by which active  $\text{BaTaO}_2\text{N}$  was formed was examined, and the high reactivity of the amorphous  $\text{Ta}_2\text{O}_5 \cdot 3\text{H}_2\text{O}$  nanoparticles was determined to be important. The use of highly reactive nanoparticles under mild nitridation conditions could allow the future development of high-performance oxynitride photocatalysts for overall water splitting.

Received 26th December 2022  
Accepted 16th February 2023

DOI: 10.1039/d2ta10010j  
[rsc.li/materials-a](http://rsc.li/materials-a)

## Introduction

Overall water splitting *via* single-step photoexcitation using particulate photocatalysts is recognized as one of the most useful means of achieving sustainable solar hydrogen production, partly because this process can be readily scaled up.<sup>1,2</sup> As an example, solar hydrogen production from water using Al-doped  $\text{SrTiO}_3$  as an ultraviolet (UV) photoresponsive powder photocatalyst has recently been demonstrated in a 100 m<sup>2</sup> system.<sup>3</sup> Even so, the development of cost-effective systems will

require particulate photocatalysts capable of driving one-step-excitation water splitting in response to visible light wavelengths of 400 to 700 nm. To date, studies regarding visible-light-driven photocatalysts have been primarily performed using (oxy)nitrides<sup>4–7</sup> and oxysulfides. Unfortunately, only a limited number of such compounds, including  $\text{TaON}$ , Zr-doped  $\text{TaON}$ ,<sup>8</sup>  $\text{Ta}_3\text{N}_5$  grown on  $\text{KTaO}_3$  (ref. 9) and  $\text{Y}_2\text{Ti}_2\text{O}_5\text{S}_2$ ,<sup>10</sup> have been reported to be photocatalytically active for overall water splitting.

Barium tantalum oxynitride,  $\text{BaTaO}_2\text{N}$ , has a narrow bandgap energy of 1.9 eV along with a robust perovskite structure, and is highly stable in water. Thus, this material is considered a promising catalyst capable of utilizing long-wavelength visible light. Significant work has been devoted over the past two decades to tuning the morphology of  $\text{BaTaO}_2\text{N}$  to obtain a material that is active for water splitting. Complete nitridation based on reaction durations longer than 10 h under a flow of gaseous  $\text{NH}_3$  at temperatures higher than 1123 K, both in the absence and presence of a flux, has been employed.  $\text{BaTaO}_2\text{N}$  obtained from these processes has been found to promote half-reactions evolving either  $\text{H}_2$  or  $\text{O}_2$  when using sacrificial reagents.<sup>6,7,11–13</sup> This material has also been applied to Z-scheme water splitting as a particulate photocatalyst for hydrogen evolution<sup>14,15</sup> in combination with  $\text{WO}_3$ . Very recently, Mg-doped  $\text{BaTaO}_2\text{N}$  was reported to be active for water splitting

<sup>a</sup>Japan Technological Research Association of Artificial Photosynthetic Chemical Process (ARPChem), 2-11-16 Yayoi, Bunkyo-ku, Tokyo 113-8656, Japan

<sup>b</sup>Research Initiative for Supra-Materials, Interdisciplinary Cluster for Cutting Edge Research, Shinshu University, Nagano-shi, Nagano 380-8553, Japan. E-mail: [domen@chemsys.t.u-tokyo.ac.jp](mailto:domen@chemsys.t.u-tokyo.ac.jp)

<sup>c</sup>Department of Chemistry, Faculty of Science Okayama University, 3-1-1 Tsusimanaka Kita-ku Okayama-shi, Okayama 700-8530, Japan

<sup>d</sup>Institute of Engineering Innovation and Department of Chemical System Engineering, School of Engineering, The University of Tokyo, Tokyo 113-8656, Japan

<sup>e</sup>Institute for Tenure Track Promotion, University of Miyazaki, Nishi 1-1 Gakuen-kibanadai, Miyazaki 889-2192, Japan

<sup>f</sup>Office of University Professors, The University of Tokyo, 2-11-16 Yayoi, Bunkyo-ku, Tokyo 113-8656, Japan

† Electronic supplementary information (ESI) available. See DOI: <https://doi.org/10.1039/d2ta10010j>

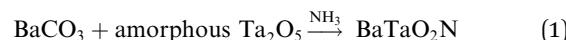


after having  $\text{Cr}_2\text{O}_3$  and Rh deposited on its surface as cocatalysts.<sup>16</sup> However, only minimal activity was observed without Mg addition. Overall water splitting has not yet been realized on pristine  $\text{BaTaO}_2\text{N}$  particulate photocatalysts, and the successful achievement of this process without the incorporation of dopants remains an important challenge.

The methods used to synthesize  $\text{BaTaO}_2\text{N}$  are now commonly based on direct nitridation of mixtures of various materials, such as barium and tantalum oxides, rather than using a barium tantalate precursor such as  $\text{Ba}_5\text{Ta}_4\text{O}_{15}$ . During the nitridation of  $\text{Ba}_5\text{Ta}_4\text{O}_{15}$  by gaseous  $\text{NH}_3$ , lattice O atoms are replaced by N atoms in conjunction with reduction by hydrogen obtained from the  $\text{NH}_3$ . However, this reaction proceeds from the surface to the interior of the catalyst particles, resulting in inhomogeneous phase formation with variations in the extent of nitridation. In contrast, the nitridation of a mixture involves a solid-phase reaction between barium and tantalum oxides that accompanies the nitridation process and generates a more homogeneous product. Consequently,  $\text{BaTaO}_2\text{N}$  exhibiting improved photocatalytic performance can be obtained. As an example, in prior work a mixture of  $\text{BaCO}_3$ ,  $\text{MgO}$  and  $\text{Ta}_2\text{O}_5$  was directly nitrided in a  $\text{RbCl}$  flux to produce active  $\text{Mg-BaTaO}_2\text{N}$ .<sup>16</sup>

Our own group previously demonstrated that amorphous  $\text{Ta}_2\text{O}_5 \cdot 3\text{H}_2\text{O}$  nanoparticles can be used as a starting material for the synthesis of  $\text{TaON}$  and Zr-doped  $\text{TaON}$  exhibiting very high activity for overall water splitting compared with materials obtained from large crystalline  $\text{Ta}_2\text{O}_5$  particles.<sup>8</sup> There are two advantages to the use of amorphous Ta complexes. Firstly, the high reactivity of these materials allows rapid nitridation at relatively low temperatures and so may prevent or at least minimize the formation of reduced  $\text{Ta}^{3+}/\text{Ta}^{4+}$  species. Secondly, smaller catalyst particles can be obtained. Thus, the use of amorphous  $\text{Ta}_2\text{O}_5$  is also an interesting approach to the synthesis of  $\text{BaTaO}_2\text{N}$  photocatalysts for overall water splitting. On this basis, in the present study,  $\text{BaTaO}_2\text{N}$  was prepared by

direct nitridation of amorphous  $\text{Ta}_2\text{O}_5$  with  $\text{BaCO}_3$  via the reaction



while varying the synthesis conditions. The process of producing active  $\text{BaTaO}_2\text{N}$  according to reaction (1) was assessed based on elucidating the various fundamental reaction paths that could take place during nitridation. The present approach is also expected to be applicable to the synthesis of other oxynitrides.

## Results and discussion

### Characterization of $\text{BaTaO}_2\text{N}$

Details regarding the preparation of  $\text{BaTaO}_2\text{N}$  are provided in the Methods section. Briefly, a white precipitate comprising amorphous  $\text{Ta}_2\text{O}_5 \cdot n\text{H}_2\text{O}$  ( $n = 3$ ; referred to herein as a- $\text{Ta}_2\text{O}_5$ ) was obtained by  $\text{H}_2\text{SO}_4$  neutralization of an alkaline solution of  $\text{Na}_3\text{TaO}_4$  in  $\text{H}_2\text{O}$ . This compound was subsequently combined with  $\text{BaCO}_3$  and then nitrided in an  $\text{NH}_3$  flow at various temperatures between 1073 and 1273 K, employing nitridation durations between 0.5 and 20 h. Fig. 1 shows X-ray diffraction (XRD) patterns for  $\text{BaTaO}_2\text{N}$  specimens prepared at 1123 K with durations from 3 to 20 h. After 3 h of nitridation, intense peaks appeared at  $2\theta = 30.7^\circ$  and  $43.9^\circ$  that were attributed to the (110) and (200) planes of  $\text{BaTaO}_2\text{N}$  having a characteristic perovskite structure. The XRD pattern for this sample also contained less intense peaks assigned to  $\text{Ta}_3\text{N}_5$  and  $\text{Ba}_5\text{Ta}_4\text{O}_{15}$  phases. After a 5 h nitridation, the peaks due to the oxide disappeared whereas those related to  $\text{Ta}_3\text{N}_5$  remained. With increasing nitridation time from 15 to 20 h, the  $\text{BaTaO}_2\text{N}$  peaks became more intense and sharp, indicating a higher degree of crystallinity, while  $\text{Ta}_3\text{N}_5$  peaks were still observed. Fig. 2 presents UV-visible diffuse reflectance spectra acquired from  $\text{BaTaO}_2\text{N}$  samples prepared at 1123 K with different nitridation

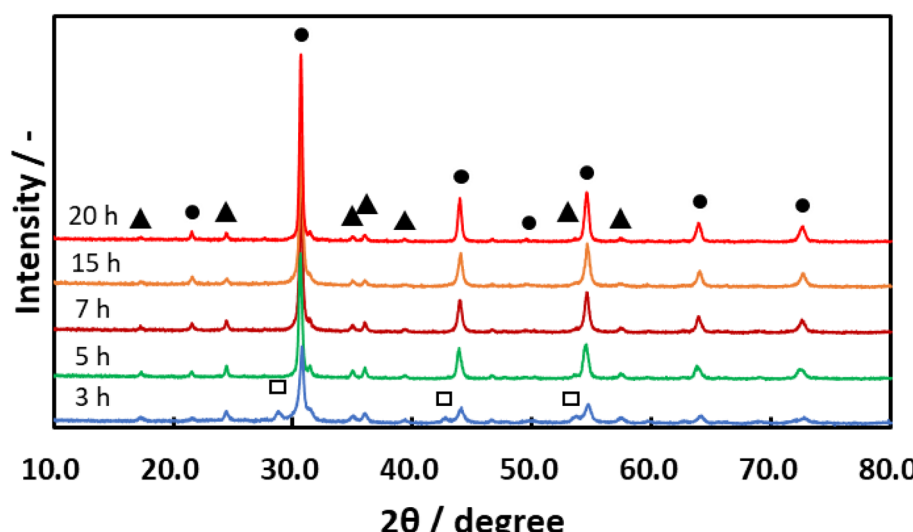


Fig. 1 X-ray diffraction patterns for  $\text{BaTaO}_2\text{N}$  prepared in a flow of  $\text{NH}_3$  at 1123 K using durations of 3–20 h. ●:  $\text{BaTaO}_2\text{N}$ , ▲:  $\text{Ta}_3\text{N}_5$ , and □:  $\text{Ba}_5\text{Ta}_4\text{O}_{15}$ .



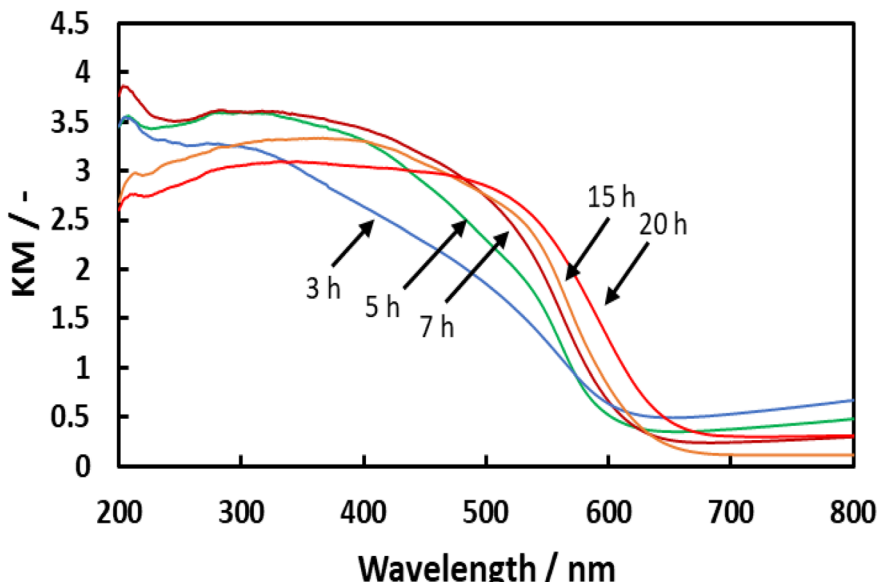


Fig. 2 UV-visible diffuse reflectance spectra obtained from  $\text{BaTaO}_2\text{N}$  prepared in a flow of  $\text{NH}_3$  at 1123 K using durations of 3–20 h.

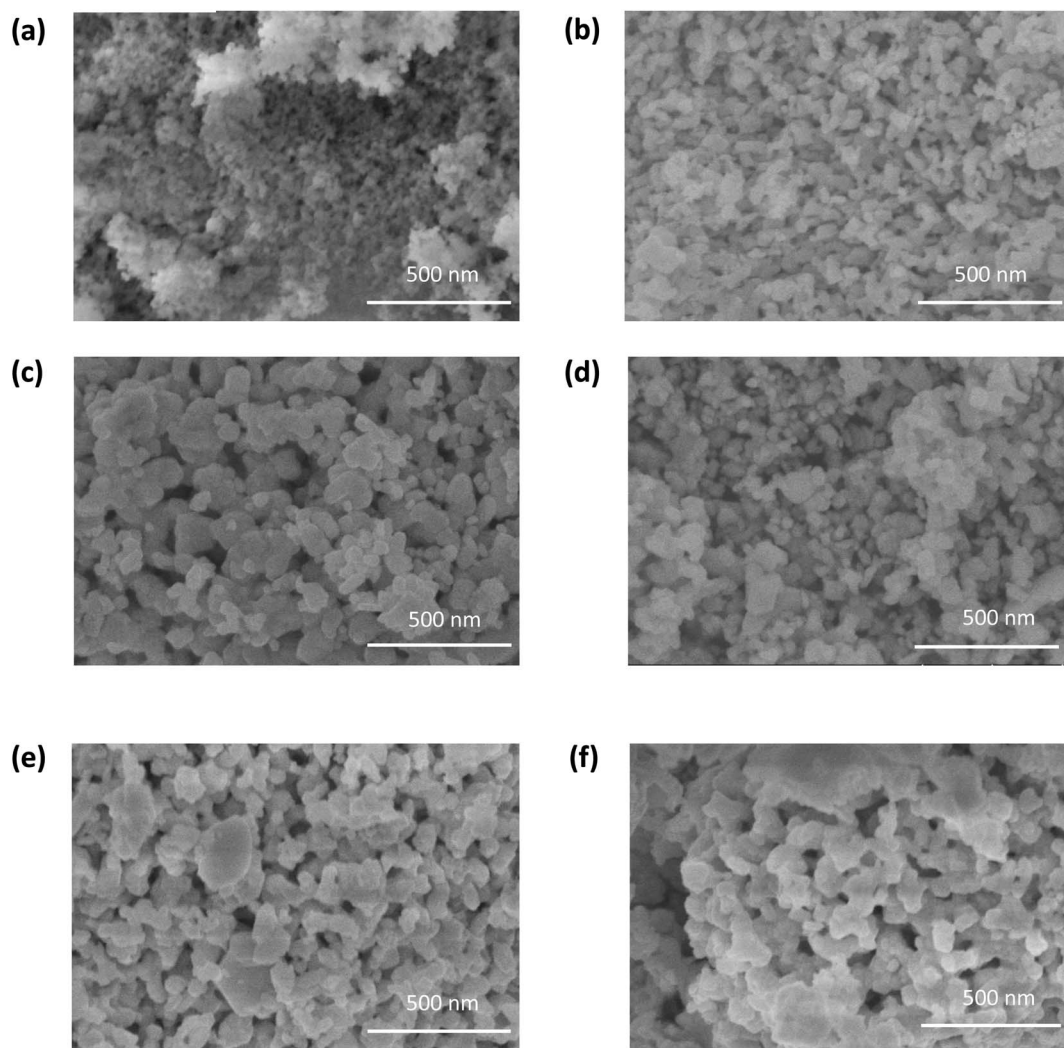


Fig. 3 SEM images of (a)  $\text{a-Ta}_2\text{O}_5$  and  $\text{BaTaO}_2\text{N}$  prepared in a flow of  $\text{NH}_3$  at 1123 K with nitridation durations of (b) 3, (c) 5, (d) 7, (e) 15 and (f) 20 h.



times. The sample treated for 3 h showed absorption that began at approximately 620 nm and increased with decreasing wavelength. Upon increasing the nitridation time to 7 h or longer, the absorption underwent a red shift. The samples nitrided for 3 and 5 h exhibited strong absorption beyond 650 nm but this absorption was reduced with increasing nitridation time. This was also associated with enhanced crystallinity of  $\text{BaTaO}_2\text{N}$ .

Fig. 3 provides the SEM images of various specimens. The original amorphous  $\text{Ta}_2\text{O}_5$  used as a raw material evidently was made of particles having a fluffy, cloud-like shape with sizes of 20–30 nm. The nitridation of this compound with  $\text{BaCO}_3$  at 1123 K produced aggregates of irregularly shaped particles roughly 50–150 nm in size. With increasing nitridation duration to 15–20 h, these irregularly shaped particles partly grew into large aggregates and connected with one another. Raising the nitridation temperature to 1173–1273 K caused the particle shape to vary and produced sintered structures (Fig. S1†). Fig. S2(a) and (b)† show the HR-TEM images of a- $\text{Ta}_2\text{O}_5$  and  $\text{BaTaO}_2\text{N}$ , respectively. In contrast to a- $\text{Ta}_2\text{O}_5$  with amorphous structural characteristics,  $\text{BaTaO}_2\text{N}$  exhibits crystalline lattice fringes.

### Water splitting reaction

Fig. 4 summarizes the extent of  $\text{H}_2\text{O}$  decomposition in response to Xe lamp illumination of a  $\text{BaTaO}_2\text{N}$  specimen nitrided at 1123 K for 5 h and loaded with Rh,  $\text{Cr}_2\text{O}_3$  and  $\text{IrO}_2$  as cocatalysts. Both  $\text{H}_2$  and  $\text{O}_2$  were generated in stoichiometric amounts during the initial stage of the reaction and the quantities of these gases increased linearly during the reaction. During the second and third runs following the evacuation of gaseous products, the gas amounts produced were nearly the same as those in the first run. The stoichiometric and constant production of  $\text{H}_2$  and  $\text{O}_2$  in these trials clearly indicates that one-step-excitation overall water splitting took place. Fig. 5 plots

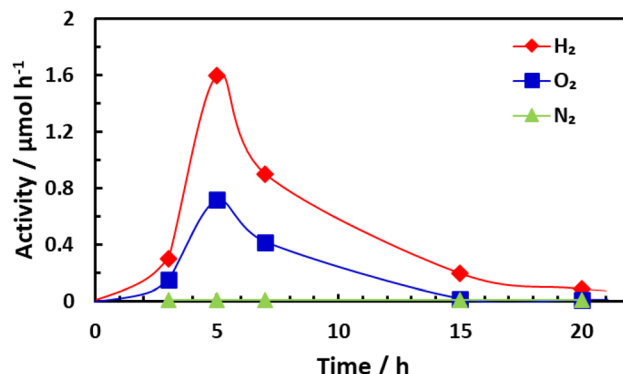


Fig. 5 Effects of nitridation time on the photocatalytic activity of  $\text{BaTaO}_2\text{N}$  during the water splitting reaction.  $\text{BaTaO}_2\text{N}$  was prepared by nitridation at 1123 K for varying durations and was loaded with 2 wt% Rh, 1 wt%  $\text{Cr}_2\text{O}_3$  and 0.3 wt%  $\text{IrO}_2$  as cocatalysts. Reaction conditions: lamp source: 300 W Xe lamp ( $\lambda > 420$  nm), reaction temperature: 288 K, and background pressure: Ar at 5 kPa.

$\text{H}_2$  and  $\text{O}_2$  production as functions of nitridation time as a means of assessing photocatalytic activity. The activity is seen to have increased sharply over the range of 3–5 h, passed through a maximum at 5 h, and then decreased over the range of 7–15 h. The  $\text{H}_2$  evolution for  $\text{BaTaO}_2\text{N}$  heated for 20 h was lower than 6% of that for 5 h and little  $\text{O}_2$  evolution was observed with this sample. The effect of the nitridation duration on the activity of  $\text{BaTaO}_2\text{N}$  after processing at 1173 or 1073 K is presented in Fig. S3 and S4,† respectively. The maximum activity appeared after 2 and 15 h at 1173 and 1073 K, respectively. Fig. S5† summarizes the changes in activity over a wide variety of nitridation times and temperatures in the form of a three-dimensional map. It is evident that lower nitridation temperatures required longer durations to achieve suitable water splitting activity. Out of this wide range of times and temperatures, the combination of 1123 K and 5 h provided the highest photocatalytic activity during overall water splitting.

As shown in Fig. 1,  $\text{BaTaO}_2\text{N}$  contained a small amount of  $\text{Ta}_3\text{N}_5$ . To avoid or at least suppress the formation of the  $\text{Ta}_3\text{N}_5$  phase, the Ba/Ta ratio for the initial mixture of  $\text{BaCO}_3$  and a- $\text{Ta}_2\text{O}_5$  was varied between 0.9 and 1.2. Fig. 6(a) shows XRD patterns for samples prepared by nitridation at 1123 K for 5 h. Peaks related to the  $\text{Ta}_3\text{N}_5$  phase remained present at a Ba/Ta ratio of 1.1 but nearly disappeared at Ba/Ta = 1.2, while peaks due to  $\text{Ba}_5\text{Ta}_4\text{O}_{15}$  appeared. The ratio of the intensity of the  $\text{Ta}_3\text{N}_5$  peaks to the  $\text{BaTaO}_2\text{N}$  peaks is plotted against the Ba/Ta ratio in Fig. 6(b), and this ratio is seen to decrease with increasing ratio. The photocatalytic activity of the catalyst (as assessed based on  $\text{H}_2$  and  $\text{O}_2$  evolution) increased beginning at Ba/Ta = 0.9 and peaked at Ba/Ta = 1, with dramatic decreases as the ratio was further increased to a value of 2 (Fig. 6(c)). A Ba/Ta ratio of 1 was determined to provide the highest activity regardless of the presence of  $\text{Ta}_3\text{N}_5$ . Although it is possible that the  $\text{Ta}_3\text{N}_5$  phase contributed to photocatalysis, the poor correlation between the amount of  $\text{Ta}_3\text{N}_5$  phase and the activity of the material suggests that this phase had only a minimal effect on the photocatalytic activity of  $\text{BaTaO}_2\text{N}$ . Water splitting trials

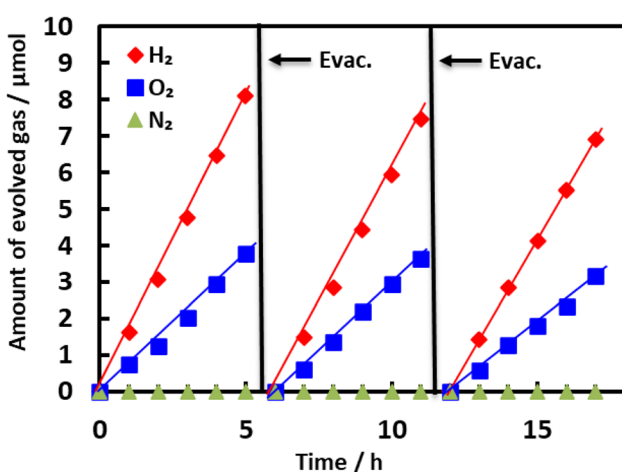


Fig. 4 Evolution of various gases over time during the water splitting reaction over Rh/ $\text{Cr}_2\text{O}_3$ / $\text{IrO}_2$ -loaded  $\text{BaTaO}_2\text{N}$  under visible light ( $\lambda > 420$  nm).  $\text{BaTaO}_2\text{N}$  was prepared by nitridation at 1123 K for 5 h and was loaded with 2 wt% Rh, 1 wt%  $\text{Cr}_2\text{O}_3$  and 0.3 wt%  $\text{IrO}_2$  as cocatalysts. Reaction conditions: lamp source: 300 W Xe lamp, reaction temperature: 288 K, and background pressure: Ar at 5 kPa.



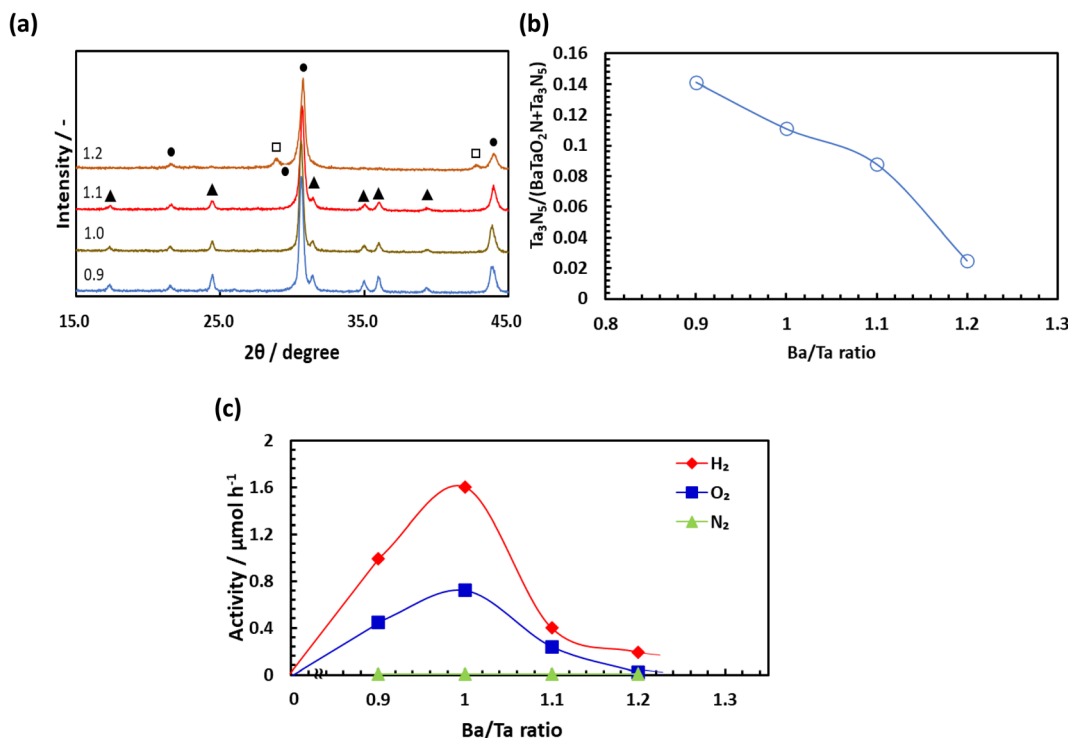


Fig. 6 (a) X-ray diffraction patterns for BaTaO<sub>2</sub>N prepared using various Ba/Ta ratios in the starting mixture, (b) the ratio of the intensity of the Ta<sub>3</sub>N<sub>5</sub> XRD peak to the sum of the intensities of the BaTaO<sub>2</sub>N and Ta<sub>3</sub>N<sub>5</sub> peaks as a function of the Ba/Ta ratio, and (c) the photocatalytic activity of Rh/Cr<sub>2</sub>O<sub>3</sub>/IrO<sub>2</sub>-loaded BaTaO<sub>2</sub>N (as reflected in the evolution of gaseous products) during the water splitting reaction as a function of the Ba/Ta ratio. BaTaO<sub>2</sub>N was prepared by nitridation at 1123 K for 5 h and was loaded with 2 wt% Rh, 1 wt% Cr<sub>2</sub>O<sub>3</sub> and 0.3 wt% IrO<sub>2</sub> as cocatalysts. Reaction conditions: lamp source: 300 W Xe lamp ( $\lambda > 420$  nm), reaction temperature: 288 K, and background pressure: Ar at 5 kPa.

were also carried out under argon at pressures of 5, 20 or 50 kPa. As shown in Fig. S6,† at least 80% of the original activity was maintained even at 50 kPa, indicating that the effect of background pressure on the photocatalytic activity was not especially strong. Fig. S7† shows changes in the amounts of H<sub>2</sub> and O<sub>2</sub> in the gas phase after turning the light irradiation off (in the dark). Their decreases were 4% for 3 h, indicating that the extent of the backward reaction from H<sub>2</sub>/O<sub>2</sub> to H<sub>2</sub>O is low.

### Effects of cocatalysts

The photocatalytic activity of the catalyst during water splitting was found to vary with changes in the amounts of Rh, Cr<sub>2</sub>O<sub>3</sub> and IrO<sub>2</sub> that were deposited. Specifically, the activity increased with increasing Rh loading up to 4 wt% (Fig. S8†). Small amounts of Cr<sub>2</sub>O<sub>3</sub> (meaning concentrations in the range of 0.5 to 1.0 wt%) were also found to lead to high photocatalytic activity (Fig. S9†). The concentration of IrO<sub>2</sub> did not have a large effect, such that even a low concentration of 0.3 wt% was sufficient to promote oxygen evolution during water splitting. Annular dark-field STEM images and STEM-EDS elemental maps were obtained to assess the states of Rh, Cr<sub>2</sub>O<sub>3</sub> and IrO<sub>2</sub> deposited on BaTaO<sub>2</sub>N. As shown in Fig. 7, the BaTaO<sub>2</sub>N particles were found to have uniform distributions of Ba, Ta, O and N. However, Rh particles on Rh/Cr<sub>2</sub>O<sub>3</sub>/IrO<sub>2</sub>-BaTaO<sub>2</sub>N were determined to form aggregates on the BaTaO<sub>2</sub>N particles while Cr<sub>2</sub>O<sub>3</sub> loaded by photodeposition were concentrated on the Rh particles. This

last result was indicative of a core–shell structure that has been previously proposed for this type of cocatalyst.<sup>1,17–19</sup> IrO<sub>2</sub> was likely to have been uniformly distributed over the BaTaO<sub>2</sub>N surface, but the evidence for this was not as clear because of the poor color pattern of the associated images, possibly owing to the low concentration of this cocatalyst.

To see the role of the cocatalysts, the water splitting reaction was tested for Rh/Cr<sub>2</sub>O<sub>3</sub>- and IrO<sub>2</sub>-loaded BaTaO<sub>2</sub>N, separately. As shown in Fig S10(a),† Rh/Cr<sub>2</sub>O<sub>3</sub>-loaded BaTaO<sub>2</sub>N was able to produce H<sub>2</sub> and O<sub>2</sub>, indicating the effectiveness of Rh/Cr<sub>2</sub>O<sub>3</sub> cocatalysts for water splitting. However, the evolution of O<sub>2</sub> was slightly low, compared to the case of Rh/Cr<sub>2</sub>O<sub>3</sub>/IrO<sub>2</sub>-loading. Fig. S10(b)† shows no activity of IrO<sub>2</sub>-loaded BaTaO<sub>2</sub>N for the water splitting reaction. From these results, it is concluded that IrO<sub>2</sub> has the ability of promoting O<sub>2</sub> evolution.

To better understand the effect of the cocatalysts on the activity, Ru was used in place of Rh, together with Cr<sub>2</sub>O<sub>3</sub> and IrO<sub>2</sub>. Fig. 8(a) shows the results for the water splitting reaction on Ru/Cr<sub>2</sub>O<sub>3</sub>/IrO<sub>2</sub>-BaTaO<sub>2</sub>N. These data demonstrate that both H<sub>2</sub> and O<sub>2</sub> were evolved and that the amounts of these gases increased in an essentially linear fashion as the irradiation time was increased. As shown in Fig. 8(b), Ru metal provided almost the same level of activity as Rh although the highest activities were obtained at 1 to 2 wt% Ru whereas 4 wt% Rh was required for optimal performance (Fig. S11†). Fig. S12† provides an annular dark-field STEM image and STEM-EDS elemental maps

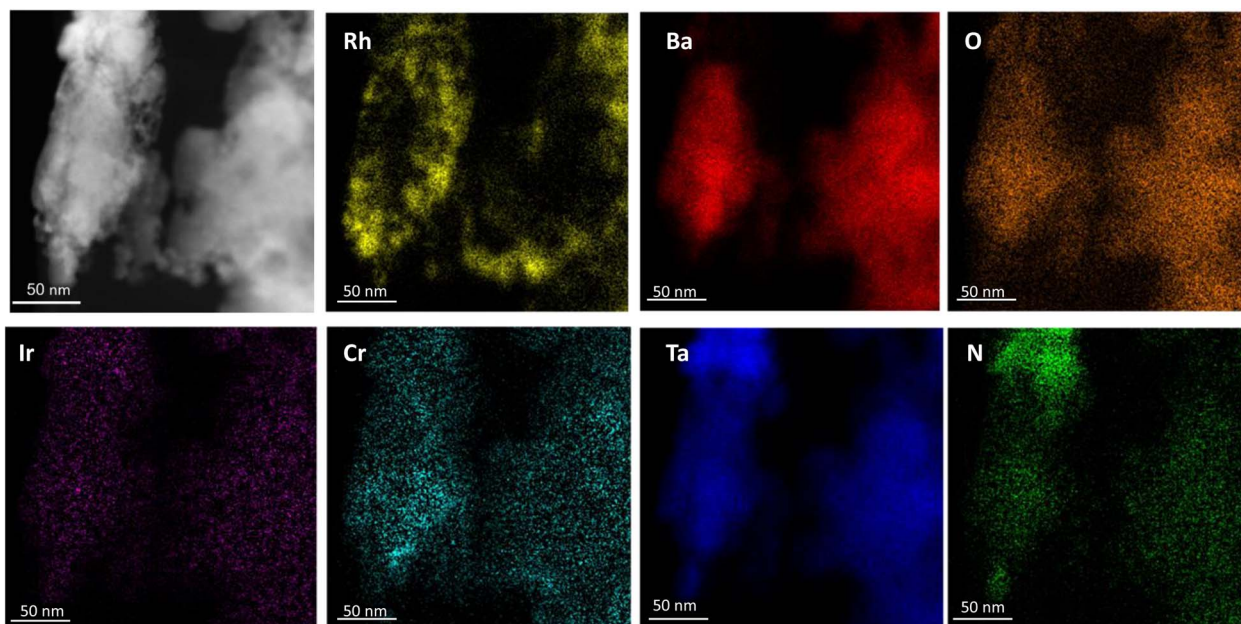


Fig. 7 Annular dark-field STEM images and STEM-EDS elemental maps for Rh/Cr<sub>2</sub>O<sub>3</sub>/IrO<sub>2</sub>-loaded BaTaO<sub>2</sub>N. BaTaO<sub>2</sub>N was prepared by nitridation at 1123 K for varying durations and was loaded with 4 wt% Rh, 1 wt% Cr<sub>2</sub>O<sub>3</sub> and 0.3 wt% IrO<sub>2</sub> as cocatalysts.

obtained from a cross-sectional sample of Ru/Cr<sub>2</sub>O<sub>3</sub>/IrO<sub>2</sub>-BaTaO<sub>2</sub>N. These results confirm that Ru metal was uniformly dispersed over BaTaO<sub>2</sub>N in the form of small particles. Thus, the difference in the amount of metal required to obtain high activity between Ru and Rh was likely related to the higher degree of dispersion of the former. Fig. S13<sup>†</sup> shows a HR-TEM image and its EDS mappings. The oval shaped Ru metal particles are attached on BaTaO<sub>2</sub>N and surrounded by a thin Cr<sub>2</sub>O<sub>3</sub> layer, which indicates the formation of a core–shell structure.

Prior to the water splitting trials, a Cr<sub>2</sub>O<sub>3</sub> layer was applied to Rh by photo-reduction of Cr<sup>6+</sup> to Cr<sup>3+</sup> using a K<sub>2</sub>CrO<sub>4</sub> solution containing 10% CH<sub>3</sub>OH as a sacrificial reagent. After Rh-loaded BaTaO<sub>2</sub>N was illuminated in an aqueous K<sub>2</sub>CrO<sub>4</sub> solution

without CH<sub>3</sub>OH, water splitting was found to proceed with the generation of stoichiometric amounts of H<sub>2</sub> and O<sub>2</sub> (Fig. S14(a)<sup>†</sup>). It should also be noted that Cr<sub>2</sub>O<sub>3</sub> could be loaded on Rh without the aid of a sacrificial reagent to produce a Cr<sub>2</sub>O<sub>3</sub>/Rh core–shell structure, after which the water splitting reaction would take place. As shown in Fig. 9, the activity increased with increasing K<sub>2</sub>CrO<sub>4</sub> concentration, and the highest activity was obtained at approximately 0.22 mM.

The effect of pH on the photocatalytic activity of Rh-loaded BaTaO<sub>2</sub>N in aqueous K<sub>2</sub>CrO<sub>4</sub> solutions was also assessed. The data in Fig. S14(b)<sup>†</sup> establish that the photocatalytic activity increased with increasing pH from 7 to 9. However, a sharp drop in activity occurred at pH 10 because Cr<sub>2</sub>O<sub>3</sub> was highly soluble

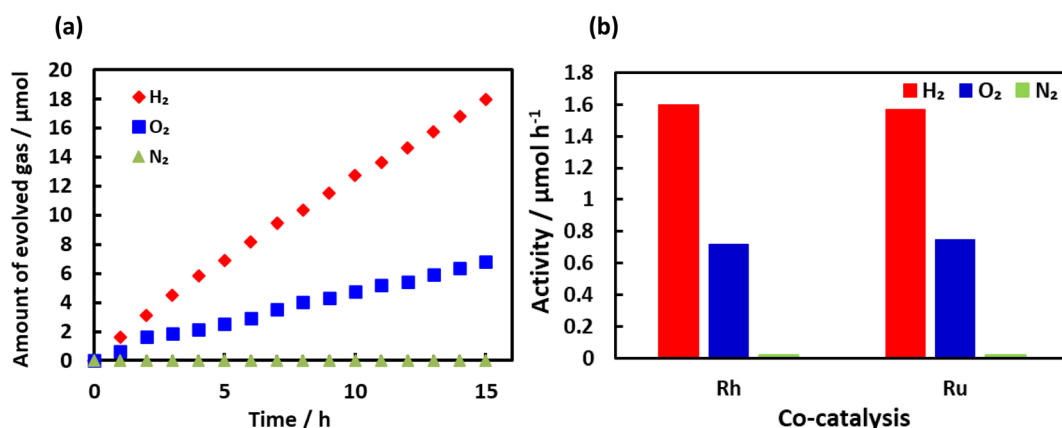


Fig. 8 (a) Evolution of gaseous products during the water splitting reaction over Ru-loaded BaTaO<sub>2</sub>N under visible light. Cocatalysts: Ru at 4 wt%, Cr<sub>2</sub>O<sub>3</sub> at 1 wt% and IrO<sub>2</sub> at 0.3 wt%. (b) Comparison of the photocatalytic activities during the water splitting reaction using Ru and Rh cocatalysts. Cocatalysts: Rh at 2 wt% or Ru at 1 wt%, Cr<sub>2</sub>O<sub>3</sub> at 0.3 wt% and IrO<sub>2</sub> at 0.3 wt%. BaTaO<sub>2</sub>N was prepared by nitridation at 1123 K for 5 h. Reaction conditions: lamp source: 300 W Xe lamp ( $\lambda > 420$  nm), reaction temperature: 288 K, and background pressure: Ar at 5 kPa.



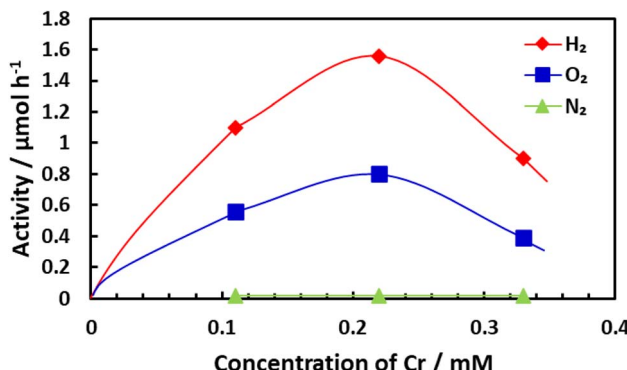


Fig. 9 Effects of the Cr concentration in aqueous solution on the photocatalytic activity of Rh-loaded  $\text{BaTaO}_2\text{N}$  during the water splitting reaction. In these trials, 2 wt% Rh-loaded  $\text{BaTaO}_2\text{N}$  was dispersed in an aqueous solution of  $\text{K}_2\text{CrO}_4$ . A concentration of 0.22 mM  $\text{K}_2\text{CrO}_4$  corresponded to a loading of 1 wt% Cr on  $\text{BaTaO}_2\text{N}$ .  $\text{BaTaO}_2\text{N}$  was prepared by nitridation at 1123 K for 5 h. Reaction conditions: lamp source: 300 W Xe lamp ( $\lambda > 420$  nm), reaction temperature: 288 K, and background pressure: Ar at 5 kPa.

in the alkaline medium. The activity enhancements observed at pH 8 and 9 were possibly related to reductions in the energy barrier to oxygen evolution with increasing  $\text{OH}^-$  concentration. This outcome is in agreement with the results obtained from previous photoelectrochemical analyses of  $\text{BaTaO}_2\text{N}$  electrodes, in which oxygen evolution was enhanced at higher pH values.<sup>20</sup>

Fig. 10 plots the apparent quantum yield (AQY) obtained from Rh/ $\text{Cr}_2\text{O}_3/\text{IrO}_2$ -loaded  $\text{BaTaO}_2\text{N}$ , together with the optical absorption of the material. The AQY at 400 nm was 0.1% but this value gradually decreased beginning at 420 nm and then dropped sharply at around 500 nm and exhibited a slower decline above 540 nm. These changes in the AQY were roughly analogous to those in optical absorption. Even though the AQY for this material was relatively low, it is noteworthy that the overall water splitting reaction proceeded at a long wavelength of 540 nm. Fig. 11 summarizes the results of the water splitting

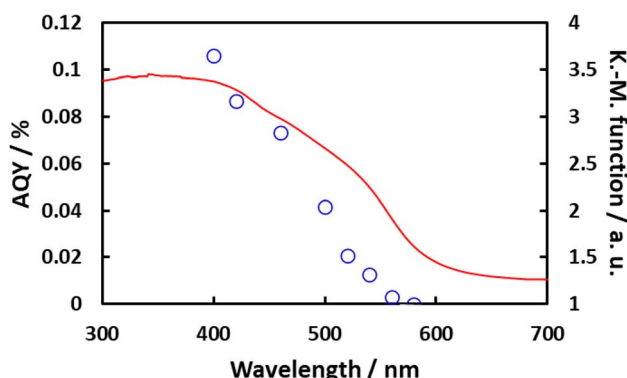


Fig. 10 AQY (○) and absorption (solid line) data for Rh/ $\text{Cr}_2\text{O}_3/\text{IrO}_2$ -loaded  $\text{BaTaO}_2\text{N}$  as a function of wavelength.  $\text{BaTaO}_2\text{N}$  was prepared by nitridation at 1123 K for 5 h and was loaded with 2 wt% Rh, 1 wt%  $\text{Cr}_2\text{O}_3$  and 0.3 wt%  $\text{IrO}_2$  as cocatalysts. Reaction conditions: lamp source: 300 W Xe lamp, reaction temperature: 288 K, and background pressure: Ar at 5 kPa.

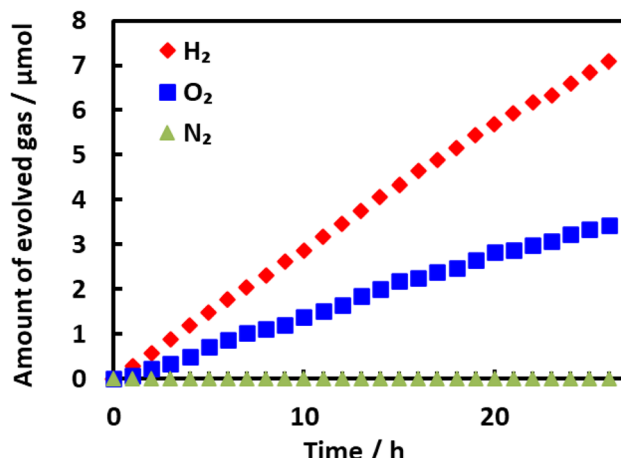


Fig. 11 Steady evolution of gaseous products during the water splitting reaction on Rh/ $\text{Cr}_2\text{O}_3/\text{IrO}_2$ -loaded  $\text{BaTaO}_2\text{N}$  under simulated light.  $\text{BaTaO}_2\text{N}$  was prepared by nitridation at 1123 K for 5 h and was loaded with 2 wt% Rh, 1 wt%  $\text{Cr}_2\text{O}_3$  and 0.3 wt%  $\text{IrO}_2$  as cocatalysts. Reaction conditions: lamp source: AM 1.5G solar radiation, reaction temperature: 288 K, and background pressure: Ar at 5 kPa.

reaction on Rh/ $\text{Cr}_2\text{O}_3/\text{IrO}_2$ - $\text{BaTaO}_2\text{N}$  when irradiated using a solar simulator. Constant generation of both  $\text{H}_2$  and  $\text{O}_2$  from  $\text{H}_2\text{O}$  was observed during prolonged irradiation and the solar-to-hydrogen (STH) yield was estimated to be  $5 \times 10^{-4}\%$ . This value is slightly higher than  $4 \times 10^{-4}\%$  reported for Mg-doped  $\text{BaTaO}_2\text{N}$ .<sup>16</sup>

### Mechanism of active $\text{BaTaO}_2\text{N}$ formation

It is important to have an understanding of the mechanism responsible for the formation of photocatalytically active  $\text{BaTaO}_2\text{N}$ . The generation of  $\text{BaTaO}_2\text{N}$  from a mixture of  $\text{BaCO}_3$  and  $\text{a-Ta}_2\text{O}_5$  in a flow of  $\text{NH}_3$  involves several parallel reaction paths, but these can be simplified by dividing them into several separate processes, as summarized in Fig. S15(a).<sup>†</sup> Here, reaction path (1) involves the rapid formation of an oxide precursor having the general formula  $\text{BaTaO}_x$  (but most likely  $\text{Ba}_5\text{Ta}_4\text{O}_{15}$ ) at increasing temperatures, followed by nitridation of this oxide. In contrast, path (2) proceeds via the selective formation of an oxynitride precursor such amorphous  $\text{BaTaO}_x\text{N}_y$  at low temperatures followed by complete nitridation. In path (3), the nitridation of  $\text{a-Ta}_2\text{O}_5$  to  $\text{TaON}$  proceeds preferentially after which reaction with  $\text{BaCO}_3$  occurs to produce  $\text{BaTaO}_2\text{N}$  in a flow of  $\text{NH}_3$ . The nitridation of  $\text{TaON}$  to  $\text{Ta}_3\text{N}_5$  readily proceeds, as demonstrated in prior work, and the reaction between  $\text{Ta}_3\text{N}_5$  and  $\text{BaCO}_3$  is a well-known oxynitride reaction in  $\text{N}_2$ .<sup>20</sup> In this process, some unreacted  $\text{Ta}_3\text{N}_5$  also remains in the product. There have been several reports that  $\text{BaCN}_2$  is formed by the nitridation of  $\text{BaCO}_3$ , but XRD peaks related to  $\text{BaCN}_2$  were not observed and so the contribution of this reaction to  $\text{BaTaO}_2\text{N}$  formation was likely negligible.<sup>21–23</sup> Reaction paths (1) to (5) were examined by synthesizing  $\text{BaTaO}_2\text{N}$  via each path, with the results presented in Fig. S15(b).<sup>†</sup> Both reaction paths (1) and (2) were found to generate  $\text{BaTaO}_2\text{N}$  that was active for overall water splitting. However, the latter showed higher activity than



the former, indicating that path (2) is superior. In contrast, the processes from path (3) to (5) resulted in the formation of inactive  $\text{BaTaO}_2\text{N}$ . The generation of highly active  $\text{BaTaO}_2\text{N}$  via reaction path (2) clearly demonstrates the importance of the reactivity of  $\text{a-Ta}_2\text{O}_5$ , which allows rapid nitridation even at low temperatures. To confirm the validity of this concept, large crystalline  $\text{Ta}_2\text{O}_5$  particles were used instead of  $\text{a-Ta}_2\text{O}_5$  for  $\text{BaTaO}_2\text{N}$  preparation using the same nitridation conditions as were applied in trials with  $\text{a-Ta}_2\text{O}_5$ . The photocatalytic activity of the resulting  $\text{BaTaO}_2\text{N}$  after  $\text{Rh/Cr}_2\text{O}_3/\text{IrO}_2$  loading was negligibly small, confirming the importance of amorphous  $\text{Ta}_2\text{O}_5$ . One of the functions of amorphous  $\text{a-Ta}_2\text{O}_5$  particles is that it has higher reactivity than crystalline  $\text{Ta}_2\text{O}_5$ , which enables  $\text{BaTaO}_2\text{N}$  synthesis at low temperatures and thus small particle formation. In addition, it is likely that the reaction with  $\text{BaCO}_3$  will proceed uniformly, compared to crystalline  $\text{Ta}_2\text{O}_5$  that consists of crystalline planes with different reactivity. These

functions of amorphous  $\text{a-Ta}_2\text{O}_5$  are thought to result in the formation of high-quality  $\text{BaTaO}_2\text{N}$ .

The plot of photocatalytic activity against nitridation time in Fig. 5 indicates that the high activity of  $\text{BaTaO}_2\text{N}$  nitrided for 5 h was greatly decreased after 15 to 20 h of nitridation. Transient absorption spectroscopy (TAS) was employed to analyze the photoexcited states of active and inactive  $\text{BaTaO}_2\text{N}$  prepared by nitridation at 5 and 20 h, respectively. The TAS data in Fig. 12(a) and (b) contain two absorption features in the range 17 000–5000  $\text{cm}^{-1}$  and below 4000  $\text{cm}^{-1}$ . These can be assigned to deeply trapped electrons and free electrons, respectively.<sup>24,25</sup> Increasing the nitridation time from 5 to 20 h drastically altered the shape of the spectrum. Specifically, the intensity of the peak related to deeply trapped electrons was significantly increased whereas that of the free electron peak decreased. These results suggest that the concentration of mid-gap states capable of deeply trapping photogenerated electrons was increased by

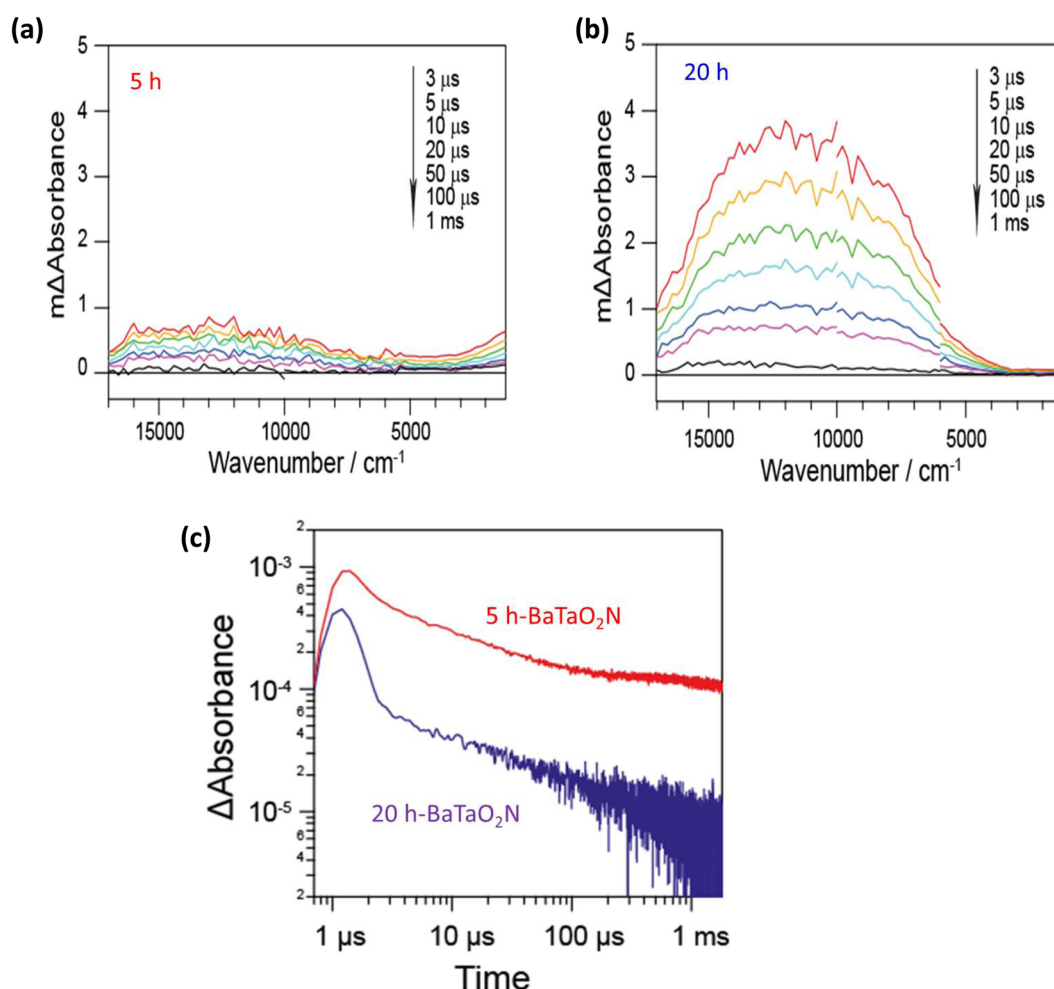


Fig. 12 (a) and (b) Time-resolved spectra and (c) decay kinetics of  $\text{BaTaO}_2\text{N}$  prepared by nitridation at 1123 K for 5 or 20 h. Active and inactive  $\text{BaTaO}_2\text{N}$  specimens were obtained by nitridation at 1123 K for 5 and 20 h, respectively (see Fig. 5). The TA spectra were obtained by scanning the probe energy from 17 000–1200  $\text{cm}^{-1}$  (0.15–2.1 eV). In the mid-IR region (6000–1200  $\text{cm}^{-1}$ ), an IR beam emitted by a  $\text{MoSi}_2$  coil was used, while, in the visible to near-IR region (17 000–6000  $\text{cm}^{-1}$ ), a probe beam generated by a halogen lamp was focused on the sample. During the acquisition of the transient decay profile of photoexcited free electrons, the absorption signal was monitored at 2000  $\text{cm}^{-1}$  (5000 nm) after irradiation with 470 nm laser pulses (fluence: 1 mJ per pulse) at a frequency of 1 Hz to achieve bandgap excitation of photocarriers in  $\text{BaTaO}_2\text{N}$ . Measurements were carried out in a  $\text{N}_2$  atmosphere at room temperature.



extending the nitridation time. Furthermore, the absorption in the region of 5000–16,000 cm<sup>−1</sup> was very low in the case of the specimen nitrided for 5 h but very high for the 20 h specimen. It is therefore evident that the number of electrons trapped in vacancies was much smaller in the former compared with the latter. Fig. 12(c) shows the TAS data obtained at 5000 nm (2000 cm<sup>−1</sup>) from samples nitrided for 5 and 20 h. The signal generated by the former material decayed very slowly and maintained a high level of intensity whereas that for the latter decayed more rapidly to a very low level. The intensity of the TA signal is correlated with the population of free electrons and so these results indicate that the 5 h specimen was able to generate long-lived free electrons. It is apparent that the active 5 h sample had a very low density of trap sites induced by defects (such as oxygen vacancies) and a high level of long-lived free electrons, both of which contributed to its excellent photocatalytic performance. Prolonged nitridation (15–20 h) increased the concentration of oxygen vacancies and other defects capable of deeply trapping photogenerated electrons.

The effect of oxygen vacancies was investigated by producing inactive BaTaO<sub>2</sub>N *via* a 15 h nitridation and then exposing this material to a N<sub>2</sub> atmosphere containing 100 ppm O<sub>2</sub> at 823 K for 2 h. As shown in Fig. S16,† the initial low photocatalytic activity was increased by a factor of 5 and H<sub>2</sub> and O<sub>2</sub> were generated in a nearly stoichiometric ratio. The incorporation of oxygen in the specimen evidently recovered its original activity. This finding provides evidence that the oxygen vacancies formed by prolonged nitridation deactivated BaTaO<sub>2</sub>N. Analyses by X-ray photoelectron spectroscopy (XPS) as presented in Fig. S17(a) and (b)† demonstrated that the intensities of the Ta 4f peaks (associated with Ta<sup>3+</sup>) were much higher in the case of BaTaO<sub>2</sub>N nitrided for 20 h compared with the 5 h specimen. Because Ta<sup>3+</sup> sites can act as recombination centers for photoexcited electrons and holes, increasing the number of these sites decreased the photocatalytic activity. Together, these TAS and XPS results confirm the exceptional performance of the photocatalytically active BaTaO<sub>2</sub>N obtained by 5 h nitridation and explain the enhanced performance of this material during the water splitting reaction.

## Conclusions

To the best of our knowledge, this work represents the first-ever demonstration of one-step-excitation overall water splitting using pristine BaTaO<sub>2</sub>N. The direct nitridation of a mixture of amorphous Ta<sub>2</sub>O<sub>5</sub> (Ta<sub>2</sub>O<sub>5</sub>·3H<sub>2</sub>O) nanoparticles and BaCO<sub>3</sub> produced a BaTaO<sub>2</sub>N photocatalyst active for overall water splitting under visible light extending to a wavelength of 540 nm following modification with Rh (or Ru), Cr<sub>2</sub>O<sub>3</sub> and IrO<sub>2</sub> as cocatalysts. The photocatalytic activity was found to be greatly affected by the concentrations of the cocatalysts, and the optimal amounts were determined to be 4 wt% (2 wt% for Ru), 1 wt% and 0.3 wt%, respectively. A wide range of nitridation conditions was examined with temperatures from 1023 to 1273 K and times from 0.5 to 20 h, and the highest activity was obtained for mild NH<sub>3</sub>-based nitridation at 1123 K for 5 h. Even though a low nitridation temperature was employed, extending

the duration to 15–20 h produced BaTaO<sub>2</sub>N with negligible activity. Analyses by TAS clearly showed that the active BaTaO<sub>2</sub>N contained the largest population of photoexcited free electrons, and that these electrons had long lifetimes owing to a small number of defects. The mechanism by which BaTaO<sub>2</sub>N was formed during NH<sub>3</sub> nitridation from the present mixture of starting materials was assessed, and the elevated reactivity of amorphous Ta<sub>2</sub>O<sub>5</sub> nanoparticles is thought to be an important aspect of this process. Although the efficiency of the photocatalysis remains very low, the concept of employing highly reactive nanoparticles shows promise and could be used in future to develop high-quality oxynitride photocatalysts.

## Methods

### Synthesis of BaTaO<sub>2</sub>N

Na<sub>3</sub>TaO<sub>4</sub> was initially prepared as a starting material for the synthesis of amorphous tantalum oxides. In this process, Ta<sub>2</sub>O<sub>5</sub> (99.99%, Rare Metal Co.) and NaOH (98%, Fujifilm Wako Pure Metal Co.) were thoroughly mixed at a Na : Ta molar ratio of 5 : 1. The mixture was then transferred to an alumina crucible and heated in air at 623 K for 12 h. The resulting solid generated an XRD pattern containing peaks attributable to Na<sub>3</sub>TaO<sub>4</sub> and to excess NaOH. This product was subsequently dissolved in H<sub>2</sub>O by sonication and stirring to produce an aqueous solution of Na<sub>8</sub>[Ta<sub>6</sub>O<sub>19</sub>] with a pH close to 13.<sup>26–28</sup> This alkaline solution was neutralized by adding H<sub>2</sub>SO<sub>4</sub> until a white precipitate was observed at pH 7 based on the protonation of [Ta<sub>6</sub>O<sub>19</sub>]<sup>8−</sup> anions followed by decomposition to produce amorphous hydrous tantalum, Ta<sub>2</sub>O<sub>5</sub>·nH<sub>2</sub>O. The precipitate was washed five times with pure water to remove residual Na<sub>2</sub>SO<sub>4</sub> and then dried overnight under vacuum at 313 K. The XRD pattern of the product confirmed its amorphous structure and the material was then converted to crystalline Ta<sub>2</sub>O<sub>5</sub> by heating in air at 1023 K. Thermogravimetric/differential thermal analysis data showed that the amorphous hydrous tantalum oxide had the formula Ta<sub>2</sub>O<sub>5</sub>·3H<sub>2</sub>O. This material is referred to herein as a-Ta<sub>2</sub>O<sub>5</sub>.

BaTaO<sub>2</sub>N was prepared by a solid state reaction. In this synthesis, BaCO<sub>3</sub> (99.99%, Rare Metallic Co.) and a-Ta<sub>2</sub>O<sub>5</sub> were thoroughly mixed in an agate mortar containing a drop of C<sub>2</sub>H<sub>5</sub>OH. The resulting mixture was placed in an alumina crucible and directly nitrided under a flow of NH<sub>3</sub> at a rate of 500 mL min<sup>−1</sup> and at various temperatures from 1023 to 1273 K with durations ranging from 0.5 to 20 h. The resulting BaTaO<sub>2</sub>N was washed with dilute HCl and water in conjunction with sonication, removed by filtration and then vacuum dried at 313 K for 2 h.

### Loading of cocatalysts on BaTaO<sub>2</sub>N

The cocatalysts were typically loaded onto BaTaO<sub>2</sub>N in the order Rh, Cr<sub>2</sub>O<sub>3</sub> and IrO<sub>2</sub>. The Rh was deposited using an impregnation method. In this process, a solution of RhCl<sub>3</sub>·3H<sub>2</sub>O (99.9%, Wako Pure Chemical Co. Ltd.) in water was added dropwise to BaTaO<sub>2</sub>N powder until incipient wetness was obtained. After drying, the powder was heated under a flow of H<sub>2</sub> (10%)/N<sub>2</sub>



(90%) at 573 K for 1 h so as to convert the Rh compound to Rh metal particles on BaTaO<sub>2</sub>N. The Rh loadings on these specimens were in the range 1 to 4 wt%. A Cr<sub>2</sub>O<sub>3</sub> layer was applied by dispersing a quantity of Rh-loaded BaTaO<sub>2</sub>N in an aqueous K<sub>2</sub>CrO<sub>4</sub> solution containing 10 vol% CH<sub>3</sub>OH as a sacrificial reagent with subsequent illumination (>350 nm) for 4 h. This procedure reduced Cr<sup>6+</sup> to Cr<sup>3+</sup> on the Rh metal surfaces to produce a core–shell structure in which Rh metal particles were covered with Cr<sub>2</sub>O<sub>3</sub>. This structure helped to suppress backward reactions involving H<sub>2</sub> and O<sub>2</sub>, as has been reported previously.<sup>17,18</sup> Following this, colloidal IrO<sub>2</sub> nanoparticles obtained from the hydrolysis of Na<sub>2</sub>IrCl<sub>6</sub> in an aqueous alkaline solution<sup>29,30</sup> were loaded onto the catalyst at a concentration of 0.3 wt%. The resulting photocatalysts are referred to herein as IrO<sub>2</sub>/Cr<sub>2</sub>O<sub>3</sub>/Rh-BaTaO<sub>2</sub>N. In the case of Ru impregnation, RuCl<sub>3</sub>·3H<sub>2</sub>O (Kanto Ltd, >95%) was used, and nearly the same procedure as that described above was applied except that the loading was in the range 0.5 to 2 wt% and the reduction temperature was 623 K.

### Water splitting reaction

Overall water splitting was performed using a closed gas circulation apparatus equipped with a gas chromatograph (GC 8 A, Shimadzu, with a thermal conductivity detector, molecular sieve 5 A column and Ar as the carrier gas). A Pyrex top-illuminated reaction vessel was connected to the reaction apparatus and used as the reactor. In each trial, a quantity of the Rh/Cr<sub>2</sub>O<sub>3</sub>/IrO<sub>2</sub>-loaded BaTaO<sub>2</sub>N photocatalyst (0.2 g) was dispersed in ultrapure water (150 mL) having a pH of approximately 7 unless otherwise specified. After complete removal of dissolved gases in the water, the reactor was filled with Ar to a background pressure of 5 kPa and then illuminated with a 300 W xenon lamp coupled with a cold mirror and a cut-off filter (L42,  $\lambda > 420$  nm) or a solar simulator (SAN-EI electronic, XRS40S1, AM 1.5G, 100 mW cm<sup>-2</sup>) with continuous agitation using a magnetic stirrer. The temperature of the reactant solution was maintained at 288 K with a flow of cooling water.

### Characterization

XRD patterns for the various samples were acquired using a Rigaku RINT-Ultima III diffractometer with a Cu K $\alpha$  radiation source. The absorption characteristics of the specimens were assessed using UV-visible diffuse reflectance spectroscopy employing a spectrophotometer (JASCO V-670DS), with Kubelka–Munk conversion of the data. Scanning transmission electron microscopy (STEM) images were obtained with a JEOL JEM-2800 instrument. Energy dispersive X-ray spectroscopy (EDS) data together with STEM images were obtained with a JEOL JEM-2800 system equipped with an Oxford Instruments X-MAX 100TLE SDD detector. XPS data were acquired using powder samples fixed on conductive carbon adhesive tape without a conductive Al pillar. Spectra were acquired with a KRATOS ULTRA2 instrument having an Al K $\alpha$  source and equipped with a charge neutralizer. The binding energy values for these spectra were calibrated based on the C 1s peak at 284.4 eV.

Microsecond-millisecond TAS analyses were performed using a pump-probe Nd:YAG laser system (Continuum, Surelite I; duration: 6 ns) equipped with custom-built spectrometers.<sup>31,32</sup> The TA spectra were obtained by scanning with probe energy from 17 000 to 1200 cm<sup>-1</sup> (0.15–2.1 eV). Photoexcited carriers in the mid-infrared (IR) region (6000–1200 cm<sup>-1</sup>) were probed using an IR beam emitted by a MoSi<sub>2</sub> coil that was applied to a film sample. The transmitted IR beam was then passed through a monochromatic grating spectrometer and to a mercury-cadmium-telluride detector (Kolmar). Photocarriers in the visible to near-IR region (17 000–6000 cm<sup>-1</sup>) were analyzed using a probe beam generated from a halogen lamp that was focused on the sample. Reflected light from the sample entered the grating spectrometer and was sent to a Si photodetector. The output electric signal was processed using an alternating current coupled amplifier (Stanford Research Systems, SR560, bandwidth: 1 MHz), and the time resolution of the spectrometer was limited to 1  $\mu$ s by the bandwidth of the amplifier. The transient decay profile for photoexcited free electrons was captured by monitoring the absorption signal at 2000 cm<sup>-1</sup> (5000 nm). The bandgap excitation of photocarriers in BaTaO<sub>2</sub>N was assessed using 470 nm laser pulses (fluence: 1 mJ per pulse) at a frequency of 1 Hz. In preparation for these analyses, a portion of the BaTaO<sub>2</sub>N powder was dispersed in water, drop-cast onto a CaF<sub>2</sub> substrate, and dried naturally in air overnight to obtain a powder film with a density of approximately 1.1 mg cm<sup>-2</sup>. Analyses were carried out in a N<sub>2</sub> atmosphere at room temperature.

### Apparent quantum yield

The AQY for one step photoexcitation overall water splitting was obtained from trials under illumination of a 300 W Xe lamp (Asahi Spectra, MAX-303) using a bandpass filter with a full width at half maximum of 15 nm. The center wavelength was varied from 400 to 480 nm in intervals of 20 nm and the number of incident photons was monitored using a diffraction grating spectroradiometer (EKO Instr. Co., LS-100). The AQY value was calculated as

$$\text{AQY (\%)} = [2 \times N(\text{H}_2)]/N(\text{photon}) \times 100,$$

where  $N(\text{H}_2)$  and  $N(\text{photon})$  are the number of H<sub>2</sub> molecules evolved and incident photons, respectively.

### Solar-to-hydrogen (STH) energy conversion efficiency

Water splitting reactions were conducted under simulated sunlight generated using a solar simulator (Sanei Electric Co., XES-40S1). The STH values were calculated as

$$\text{STG (\%)} = (R(\text{H}_2) \times \Delta G)/(I \times A) \times 100$$

where  $R(\text{H}_2)$ ,  $\Delta G$ ,  $I$  and  $A$  are the rate of hydrogen evolution (the number of H<sub>2</sub> molecules h<sup>-1</sup>) during the overall water splitting reaction, the Gibbs energy of the reaction producing gaseous hydrogen and oxygen from liquid water (237 kJ mol<sup>-1</sup> at 298 K), the energy intensity (80 mW cm<sup>-2</sup>) of the AM 1.5G solar



radiation employed (equivalent to 0.8 sun), and the illuminated sample area ( $38.5\text{ cm}^2$ ), respectively.

## Conflicts of interest

There are no conflicts to declare.

## Acknowledgements

This study was financially supported by the Artificial Photosynthesis Project (ARPChem) of the New Energy and Industrial Technology Development organization (NEDO).

## References

- 1 S. Chen, T. Takata and K. Domen, Particulate photocatalysts for overall water splitting, *Nat. Rev. Mater.*, 2017, **2**, 17050.
- 2 T. Hisatomi and K. Domen, Reaction systems for solar hydrogen production *via* water splitting with particulate semiconductor photocatalysts, *Nat. Catal.*, 2019, **2**, 387–399.
- 3 H. Nishiyama, T. Yamada, M. Nakabayashi, Y. Maehara, M. Yamaguchi, Y. Kuromiya, Y. Nagatsuma, H. Tokudome, S. Akiyama, T. Watanaba, R. Narushima, S. Okunaka, N. Shibata, T. Takata, T. Hisatomi and K. Domen, Photocatalytic solar hydrogen production from water on a 100-m<sup>2</sup> scale, *Nature*, 2021, **598**, 304–307.
- 4 C. Pan, T. Takata and K. Domen, Overall Water Splitting on the Transition-Metal Oxynitride Photocatalyst  $\text{LaMg}_{1/3}\text{Ta}_{2/3}\text{O}_2\text{N}$  over a Large Portion of the VisibleLight Spectrum, *Chem.-Eur. J.*, 2016, **22**, 1854–1862.
- 5 C. Pan, T. Takata, M. Nakabayashi, T. Masumoto, N. Shibata, Y. Ikuhara and K. Domen, A Complex Perovskite-Type Oxynitride: The First Photocatalyst for Water Splitting Operable at up to 600 nm, *Angew. Chem., Int. Ed.*, 2015, **54**, 2955–2959.
- 6 K. Ueda, T. Minegishi, J. Clune, M. Nakabayashi, T. Hisatomi, H. Nishiyama, M. Katayama, N. Shibata, J. Kubota, T. Yamada and K. Domen, Photoelectrochemical Oxidation of Water Using  $\text{BaTaO}_2\text{N}$  Photoanodes Prepared by Particle Transfer Method, *J. Am. Chem. Soc.*, 2015, **137**, 2227–2230.
- 7 H. Okamoto, M. Kodera, T. Hisatomi, M. Katayama, T. Minegishi and K. Domen, Effects of annealing conditions on the oxygen evolution activity of a  $\text{BaTaO}_2\text{N}$  photocatalyst loaded with cobalt species, *Catal. Today*, 2020, **354**, 204–210.
- 8 J. Xiao, S. Nishimae, J. Vequizo, M. Nakabayashi, T. Hisatomi, H. Li, L. Lin, N. Shibata, A. Yamakata, Y. Inoue and K. Domen, Enhanced Overall Water Splitting by a Zirconium-Doped TaON-Based Photocatalyst, *Angew. Chem., Int. Ed.*, 2022, **61**, e2021165.
- 9 Z. Wang, Y. Inoue, T. Hisatomi, R. Ishikawa, Q. Wang, T. Takata, S. Chen, N. Shibata, Y. Ikuhara and K. Domen, Overall water splitting by  $\text{Ta}_3\text{N}_5$  nanorod single crystals grown on the edges of  $\text{KTaO}_3$  particles, *Nat. Catal.*, 2018, **1**, 756–763.
- 10 Q. Wang, M. Nakabayashi, T. Hisatomi, S. Sun, S. Akiyama, Z. Wang, Z. Pan, X. Xiao, T. Watanabe, T. Yamada, N. Shibata, T. Takata and K. Domen, Oxysulfide photocatalyst for visible-lightdriven overall water splitting, *Nat. Mater.*, 2019, **18**, 827–832.
- 11 M. Hojamberdiev, K. Yabuta, J. J. M. Vequizo, A. Yamakata, S. Oishi, K. Domen and K. Teshima,  $\text{NH}_3$ -Assisted Flux Growth of Cube-like  $\text{BaTaO}_2\text{N}$  Submicron Crystals in a Completely Ionized Nonaqueous High-Temperature Solution and Their Water Splitting Activity, *Cryst. Growth Des.*, 2015, **15**, 4663–4671.
- 12 H. Li, D. Lu, S. Chen, T. Hisatomi, J. Vequizo, J. Xiao, Z. Wang, L. Lin, Q. Xiao, Y. Sun, Y. Miseki, K. Sayama, A. Yamakata, T. Takata and K. Domen, A Na-containing Pt cocatalyst for efficient visible-light-induced hydrogen evolution on  $\text{BaTaO}_2\text{N}$ , *J. Mater. Chem. A*, 2021, **9**, 13851–13854.
- 13 M. Higashi, Y. Yamanaka, O. Tomita and R. Abe, Fabrication of cation-doped  $\text{BaTaO}_2\text{N}$  photoanodes for efficient photoelectrochemical water splitting under visible light irradiation, *APL Mater.*, 2015, **3**, 104418.
- 14 Z. Wang, Y. Luo, T. Hisatomi, J. Vequizo, S. Suzuki, S. Chen, M. Nakabayashi, L. Lin, Z. Pan, N. Kariya, A. Yamakata, N. Shibata, T. Takata, K. Teshima and K. Domen, Sequential cocatalyst decoration on  $\text{BaTaO}_2\text{N}$  towards highly-active Z-scheme water splitting, *Nat. Commun.*, 2021, **12**, 1005.
- 15 M. Higashi, R. Abe, T. Takata and K. Domen, Photocatalytic Overall Water Splitting under Visible Light Using  $\text{ATaO}_2\text{N}$  (A=Ca, Sr, Ba) and  $\text{WO}_3$  in a  $\text{IO}_3^-/\text{I}^-$  Shuttle Redox Mediated System, *Chem. Mater.*, 2009, **21**, 1543–1549.
- 16 H. Li, J. Xiao, J. J. M. Vequizo, T. Hisatomi, M. Nakabayashi, Z. Pan, N. Shibata, A. Yamakata, T. Takata and K. Domen, One-Step Excitation Overall Water Splitting over a Modified Mg-Doped  $\text{BaTaO}_2\text{N}$  Photocatalyst, *ACS Catal.*, 2022, **12**, 10179–10185.
- 17 K. Maeda, K. Teramura, D. Lu, N. Saito, Y. Inoue and K. Domen, Roles of  $\text{Rh/Cr}_2\text{O}_3$  (Core/Shell) Nanoparticles Photodeposited on Visible-Light-Responsive  $(\text{Ga}_{1-x}\text{Zn}_x)(\text{N}_{1-x}\text{O}_x)$  Solid Solutions in Photocatalytic Overall Water Splitting, *J. Phys. Chem. C*, 2007, **111**, 7554–7560.
- 18 T. Takata, J. Jiang, Y. Sakata, M. Nakabayashi, N. Shibata, V. Nandal, K. Seki, T. Hisatomi and K. Domen, Photocatalytic water splitting with a quantum efficiency of almost unity, *Nature*, 2020, **581**, 411–414.
- 19 M. Yoshida, K. Takanabe, K. Maeda, A. Ishikawa, J. Kubota, Y. Sakata, Y. Ikezawa and K. Domen, Role and Function of Noble-Metal/Cr-Layer Core/Shell Structure Cocatalysts for Photocatalytic Overall Water Splitting Studied by Model Electrodes, *J. Phys. Chem. C*, 2009, **113**, 10151–10157.
- 20 S. Nishimae, Y. Mishima, H. Nishiyama, Y. Sasaki, M. Nakabayashi, Y. Inoue, M. Katayama and K. Domen, Fabrication of  $\text{BaTaO}_2\text{N}$  Thin Films by Interfacial Reactions of  $\text{BaCO}_3/\text{Ta}_3\text{N}_5$  Layers on a Ta Substrate and Resulting High Photoanode Efficiencies During Water Splitting, *Sol. RRL*, 2020, **4**, 1900542.



21 Y. Masubuchi, S. Nishitani, A. Hosono, Y. Kitagawa, J. Ueda, S. Tanabe, H. Yamane, M. Higuchi and S. Kikkawa, Red-emission over a wide range of wavelength at various temperatures from tetragonal  $\text{BaCN}_2:\text{Eu}^{2+}$ , *J. Mater. Chem. C*, 2018, **6**, 6370.

22 A. Hosono, Y. Masubuchi, T. Endo and S. Kikkawa, Molten  $\text{BaCN}_2$  for the sintering and crystal growth of dielectric oxynitride perovskite  $\text{Sr}_{1-x}\text{Ba}_x\text{TaO}_2\text{N}$  ( $x = 0.04\text{--}0.23$ ), *Dalton Trans.*, 2017, **46**, 16837.

23 A. Hosono, R. P. Stoffel, Y. Masubuchi, R. Dronkowski and S. Kikkawa, Melting Behavior of Alkaline-Earth Metal Carbodiimides and Their Thermochemistry from First-Principles, *Inorg. Chem.*, 2019, **58**, 8938–8942.

24 A. Yamakata, M. Yoshida, J. Kubota, M. Osawa and K. Domen, Potential-Dependent Recombination Kinetics of Photogenerated Electrons in n- and p- Type  $\text{GaN}$  Photoelectrodes Studied by Time-Resolved IR Absorption Spectroscopy, *J. Am. Chem. Soc.*, 2011, **133**, 11351–11357.

25 J. J. Vequizo, S. Nishioka, J. Hyodo, Y. Yamazaki, K. Maeda and A. Yamakata, Crucial impact of reduction on the photocarrier dynamics of  $\text{SrTiO}_3$  powders studied by transient absorption spectroscopy, *J. Mater. Chem. A*, 2019, **7**, 26139–26146.

26 W. H. Nelson and R. S. Tobias, Structure of the Polyanions of the Transition Metals in Aqueous Solution: The Hexatantalate, *Inorg. Chem.*, 1963, **2**, 985–992.

27 M. Filowitz, R. K. C. Ho, W. G. Klemperer and W. Shum, Oxygen-17 nuclear magnetic resonance spectroscopy of polyoxometalates. 1. Sensitivity and resolution, *Inorg. Chem.*, 1979, **18**, 93–103.

28 S. Yamazoe, K. Shibata, K. Kato and T. Wada, Needle-like  $\text{NaNbO}_3$  Synthesis via  $\text{Nb}_6\text{O}_{19}^{8-}$  Cluster Using  $\text{Na}_3\text{NbO}_4$  Precursor by Dissolution–Precipitation Method, *Chem. Lett.*, 2013, **42**, 380–382.

29 M. Hara, C. C. Waraksa, J. T. Lean, B. A. Lewis and T. E. Mallouk, Photocatalytic water oxidation in a buffered tris(2,2'-bipyridyl)ruthenium complex-colloidal  $\text{IrO}_2$  system, *J. Phys. Chem. A*, 2000, **104**, 5275–5280.

30 A. Ishikawa, T. Takata, J. N. Kondo, M. Hara, H. Kobayashi and K. Domen, Oxysulfide  $\text{Sm}_2\text{Ti}_2\text{S}_2\text{O}_5$  as a Stable Photocatalyst for Water Oxidation and Reduction under Visible Light Irradiation ( $\lambda \leq 650$  nm), *J. Am. Chem. Soc.*, 2002, **124**, 13547.

31 J. J. M. Vequizo, H. Matsunaga, T. Ishiku, S. Karnimura, T. Ohno and A. Yamakata, Trapping-Induced Enhancement of Photocatalytic Activity on Brookite  $\text{TiO}_2$  Powders: Comparison with Anatase and Rutile  $\text{TiO}_2$  Powders, *ACS Catal.*, 2017, **7**, 2644–2651.

32 J. D. Xiao, J. J. M. Vequizo, T. Hisatomi, J. Rabeh, M. Nakabayashi, Z. Wang, Q. Xiao, H. H. Li, Z. H. Pan, M. Krause, N. Yin, G. Smith, N. Shibata, A. Bruckner, A. Yamakata, T. Takata and K. Domen, Simultaneously Tuning the Defects and Surface Properties of  $\text{Ta}_3\text{N}_5$  Nanoparticles by Mg-Zr Codoping for Significantly Accelerated Photocatalytic  $\text{H}_2$  Evolution, *J. Am. Chem. Soc.*, 2021, **143**, 10059–10064.

